

Effects of anharmonic vibration on large-angle quasi-elastic scattering of $^{16}\text{O}+^{144}\text{Sm}$

Muhammad Zamrun F.* and K. Hagino†

Department of Physics, Tohoku University, Sendai 980-8578, Japan

(Dated: January 4, 2019)

We study the effects of double octupole and quadrupole phonon excitations in the ^{144}Sm nucleus on quasi-elastic $^{16}\text{O}+^{144}\text{Sm}$ scattering at backward angles. To this end, we use the coupled-channels framework, taking into account explicitly the anharmonicities of the vibrations. We use the same coupling scheme as that previously employed to explain the experimental data of sub-barrier fusion cross sections for the same system. We show that the experimental data for the quasi-elastic cross sections are well reproduced in this way, although the quasi-elastic barrier distribution has a distinct high energy peak which is somewhat smeared in the experimental barrier distribution. We also discuss the effects of proton transfer on the quasi-elastic barrier distribution. Our study indicates that the fusion and quasi-elastic barrier distributions for this system cannot be accounted for simultaneously with the standard coupled-channels approach.

PACS numbers: 24.10.Eq, 25.60.Pj, 25.70.Bc, 27.60.+j

I. INTRODUCTION

The effect of channel coupling, that is, couplings of the relative motion between the colliding nuclei to their intrinsic motions as well as transfer reactions, have been well known in heavy-ion collisions around the Coulomb barrier. In heavy-ion fusion reactions at sub-barrier energies, the channel coupling effects enhance considerably the fusion cross sections as compared to the prediction of potential model calculation [1, 2, 3]. It has been well established by now that the channel coupling gives rise to a distribution of potential barriers [4, 5, 6]. Based on this idea, a method was proposed to extract barrier distributions directly from experimental fusion excitation functions by taking the second derivative of the product of center mass energy, E , and the fusion cross section, $\sigma_{\text{fus}}(E)$, with respect to E [7]. Coupled-channels calculations as well as high precision fusion data have shown that the fusion barrier distributions, $D^{\text{fus}} = d^2[E\sigma_{\text{fus}}(E)]/dE^2$, is sensitive to the details of channel couplings, while the sensitivity is much more difficult to see in the fusion cross sections [3, 8, 9].

Similar information as the fusion cross section can also be obtained from the quasi-elastic scattering (a sum of elastic, inelastic and transfer processes) at backward angles [10]. Timmers *et al.* measured the quasi-elastic scattering cross section for several systems [11], for which the fusion barrier distribution had already been extracted [9]. They proposed that the corresponding barrier distribution can be extracted by taking the first derivative of the ratio of the quasi-elastic to the Rutherford cross sections, $d\sigma_{\text{qel}}/d\sigma_R$, with respect to the energy, E , *i.e.*, $D^{\text{qel}} = -d(d\sigma_{\text{qel}}/d\sigma_R)/dE$. The properties of the quasi-elastic barrier distributions have been studied in more details in Ref. [12]. These studies show that the quasi-

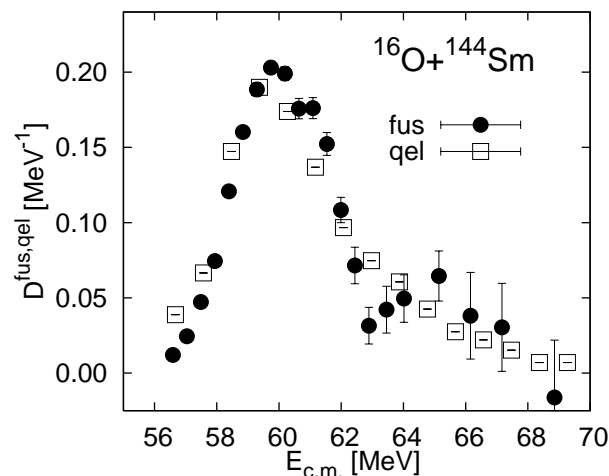


FIG. 1: Comparison between the experimental fusion (the filled circles) and quasi-elastic (the open squares) barrier distributions for the $^{16}\text{O}+^{144}\text{Sm}$ reaction. They are normalized to unit area in the energy interval between $E_{\text{c.m.}} = 56$ and 70 MeV. The experimental data are taken from Refs. [9] and [11].

elastic barrier distribution is similar to the fusion barrier distribution, although the former is somewhat smeared and less sensitive to the nuclear structure effects.

One of the systems which Timmers *et al.* measured is $^{16}\text{O}+^{144}\text{Sm}$ [11]. Figure 1 shows the comparison of the experimental barrier distribution extracted from fusion (the filled circles) and quasi-elastic (the open squares) processes. In order to compare the two barrier distributions, we scale them so that the energy integral between $E_{\text{c.m.}} = 56$ and 70 MeV is unity. For energies below 62 MeV, the two barrier distributions resemble each other. However, at higher energies, they behave rather differently, although the overall width of the distributions is similar to each other. That is, the quasi-elastic barrier distribution decreases monotonically as a function of en-

*Electronic address: zamrun@nucl.phys.tohoku.ac.jp

†Electronic address: hagino@nucl.phys.tohoku.ac.jp

ergy while the fusion barrier distribution exhibits a distinct peak at energy around $E_{c.m.} = 65$ MeV. So far, no theoretical calculations have succeeded in explaining this difference. The coupled-channels calculations of Timmers *et al.* [11] with the computer code ECIS [13], which took into account the one quadrupole, 2^+ , and the one octupole, 3^- , phonon excitations of ^{144}Sm , were unable to reproduce both the experimental data of the quasi-elastic cross sections and the quasi-elastic barrier distribution. The ECIS results for the ratio of quasi-elastic scattering to the Rutherford cross sections fall off more steeply than the experimental data, while the obtained barrier distribution has a secondary peak similar to the fusion barrier distribution. They argued that this failure is largely due to the residual excitations not included in the ECIS calculations, which they postulated to be transfer channels. Esbensen and Buck have also performed the coupled-channels calculations for this system taking into account the second order couplings [14]. However, they did not analyze the quasi-elastic barrier distribution.

These previous coupled-channels calculations took into account only the single phonon excitations in ^{144}Sm . On the other hand, Hagino *et al.* [15, 16] have shown that the double anharmonic quadrupole and octupole phonon excitations play an important role in reproducing the experimental fusion barrier distribution for this system. However, its effect on the quasi-elastic scattering has not yet been clarified so far. The aim of this paper is then to study whether the double anharmonic vibrational excitations of the ^{144}Sm nucleus can explain the difference in the shape of barrier distribution between fusion and quasi-elastic. The role of proton transfer reactions in this system is also discussed.

The paper is organized as follows. In the next section, we briefly explain the coupled-channels formalism which takes into account the anharmonicities of the vibrational excitations. We present the results of our calculations in Sec. III. We then summarize the paper in Sec. IV.

II. COUPLED-CHANNELS FORMALISM FOR ANHARMONIC VIBRATION

In this section, we briefly describe the coupled-channels formalism which includes the effects of anharmonic exci-

tations of the vibrational states. We follow the procedure of Refs. [15, 16], which was successfully applied to describe the experimental fusion cross sections as well as the fusion barrier distributions of $^{16}\text{O}+^{144,148}\text{Sm}$ systems. The total Hamiltonian of the system is assumed to be

$$H = -\frac{\hbar^2}{2\mu}\nabla^2 + H_{\text{vib}} + V_{\text{coup}}(\mathbf{r}, \xi) \quad (1)$$

where \mathbf{r} is the coordinate of the relative motion between the target and the projectile nuclei, μ is the reduced mass and ξ represents the internal vibrational degrees of freedom of the target nucleus. H_{vib} describes the vibrational spectra in the target nucleus.

The coupling between the relative motion and the intrinsic motion of the target nucleus is described by the coupling potential V_{coup} in Eq.(1), which consists of the Coulomb and nuclear parts. Using the no-Coriolis (iso-centrifugal) approximation [2, 17], they are given as

$$V_{\text{coup}}(r, \xi) = V_C(r, \xi) + V_N(r, \xi), \quad (2)$$

$$V_C(r, \xi) = \frac{Z_P Z_T e^2}{r} \left(1 + \frac{3R_T^2}{5r^2} \frac{\hat{O}_{20}}{\sqrt{4\pi}} + \frac{3R_T^3}{7r^3} \frac{\hat{O}_{30}}{\sqrt{4\pi}} \right), \quad (3)$$

$$V_N(r, \xi) = \frac{-V_0}{\left[1 + \exp \left(\frac{[r - R_0 - R_T(\hat{O}_{20} + \hat{O}_{30})/\sqrt{4\pi}]}{a} \right) \right]}. \quad (4)$$

Here \hat{O}_{20} and \hat{O}_{30} are the excitation operators for the quadrupole and octupole vibrations, respectively, and R_T is the target radius. The effect of anharmonicities for the quadrupole and octupole vibrations are taken into account based on the U(5) limit of the Interacting Boson Model (IBM). The matrix elements of the operator $\hat{O} = \hat{O}_{20} + \hat{O}_{30}$ in Eqs.(3) and (4) then read [15, 16, 18],

$$O_{ij} = \begin{bmatrix} 0 & \beta_2 & \beta_3 & 0 & 0 & 0 \\ \beta_2 & -\frac{2}{\sqrt{14N}}\chi_2\beta_2 & -\frac{2}{\sqrt{15N}}\chi_3\beta_3 & \sqrt{2(1-1/N)}\beta_2 & \sqrt{1-1/N}\beta_3 & 0 \\ \beta_3 & -\frac{2}{\sqrt{15N}}\chi_3\beta_3 & -\frac{2}{\sqrt{21N}}\chi_2\beta_2 & 0 & \sqrt{1-1/N}\beta_2 & \sqrt{2(1-1/N)}\beta_3 \\ 0 & \sqrt{2(1-1/N)}\beta_2 & 0 & -\frac{4}{\sqrt{14N}}\chi_2\beta_2 & -\sqrt{\frac{8}{15N}}\chi_3\beta_3 & 0 \\ 0 & \sqrt{1-1/N}\beta_3 & \sqrt{1-1/N}\beta_3 & -\sqrt{\frac{8}{15N}}\chi_3\beta_3 & (-\frac{2}{\sqrt{14N}}\chi_2 - \frac{2}{\sqrt{21N}}\chi_2\beta_2)\beta_2 & -\sqrt{\frac{8}{15N}}\chi_3\beta_3 \\ 0 & 0 & \sqrt{2(1-1/N)}\beta_3 & 0 & -\sqrt{\frac{8}{15N}}\chi_3\beta_3 & -\frac{4}{\sqrt{21N}}\chi_2\beta_2 \end{bmatrix} \quad (5)$$

for 6 low-lying states ($i, j=1-6$), where $|1\rangle = |0^+\rangle$, $|2\rangle = |2^+\rangle$, $|3\rangle = |3^-\rangle$, $|4\rangle = |2^+ \otimes 2^+\rangle$, $|5\rangle = |2^+ \otimes 3^-\rangle$, and $|6\rangle = |3^- \otimes 3^-\rangle$. In Eq.(5), β_2 and β_3 are the quadrupole and the octupole deformation parameters, respectively, which can be estimated from the electric transition probabilities. The scaling of coupling strength with \sqrt{N} , N being the number of boson in the system, is introduced to ensure the equivalence between the IBM and the geometric model in the large N limit [18]. When all the χ parameters in Eq.(5) are set to be zero then the quadrupole moment of all the states vanishes, and one obtains the harmonics limit in the large N limit. Nonzero values of χ generate the quadrupole moments, and, together with finite boson number, they are responsible for the anharmonicities in the vibrational excitations.

III. $^{16}\text{O}+^{144}\text{Sm}$ REACTION : COMPARISON WITH EXPERIMENTAL DATA

We now apply the formalism to analyze the quasi-elastic scattering data of $^{16}\text{O}+^{144}\text{Sm}$ [11]. The calculations are performed with a version [19] of the coupled-channels code CCFULL [17] once the coupling matrix elements are determined from Eq.(5). Notice that the isocentrifugal approximation employed in this code works well for quasi-elastic scattering at backward angles [12]. In the code, the regular boundary condition is imposed at the origin instead of the incoming wave boundary condition.

A. Effect of anharmonicities of nuclear vibrations

In the calculations presented below, we include only the excitations in the ^{144}Sm nucleus whilst the excitations of the ^{16}O is not explicitly included. For sub-barrier fusion reactions, the latter has been shown to lead only to a shift of the fusion barrier distribution in energy without significantly altering its shape [20], and hence can be incorporated in the choice of the bare potential. This is a general feature for reactions with the ^{16}O as a projectile. We have confirmed that it is the case also for the quasi-elastic barrier distribution. That is, although the ^{16}O excitations contribute to the absolute value of quasi-elastic cross sections themselves, the shape of quasi-elastic barrier distribution is not altered much. Since we are interested mainly in the difference of the shape between the fusion and the quasi-elastic barrier distributions, we simply do not include the ^{16}O excitations and instead adjust the inter-nuclear potential.

For simplicity, we take the eigenvalues of the H_{vib} in Eq.(1) to be $\epsilon = n_2\epsilon_2 + n_3\epsilon_3$, where n_2 and n_3 are the number of quadrupole and octupole phonons, respectively. ϵ_2 and ϵ_3 are the excitation energies of the quadrupole and the octupole phonon states of the target nucleus, *i.e.*, $\epsilon_2 = 1.61$ MeV and $\epsilon_3 = 1.81$ MeV, respectively. Notice that we assume the harmonic spectra

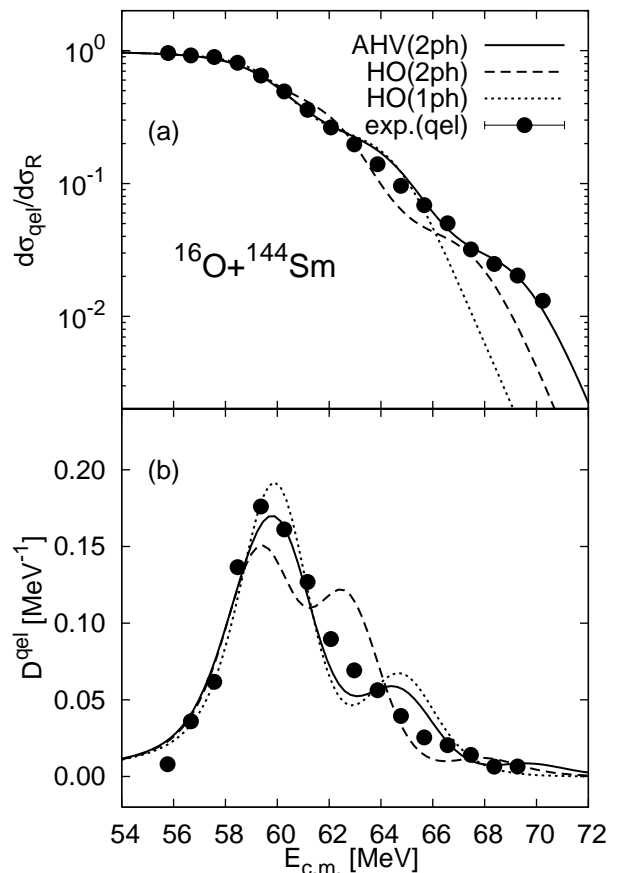


FIG. 2: Comparison of the experimental data with the coupled-channels calculations for $^{16}\text{O}+^{144}\text{Sm}$ reaction for (a) the ratio of quasi-elastic to the Rutherford cross sections and for (b) quasi-elastic barrier distribution. The dotted and dashed lines are obtained by including up to the single and the double phonon excitations in the harmonic limit, respectively. The solid line is the result of the coupled-channels calculations with the double anharmonic phonon excitations. The experimental data are taken from Ref. [11].

for the phonon excitations. It has been shown in Refs. [15, 16] that the effect of anharmonicity with respect to the excitation energy on the barrier distribution is insignificant once the energy of the single phonon states is fixed. The radius and diffuseness parameters of the real part of the nuclear potential are taken to be the same as those in Ref. [15], *i.e.*, $r_0 = 1.1$ fm and $a = 0.75$ fm, respectively, while the depth parameter is slightly adjusted in order to reproduce the experimental quasi-elastic cross sections. The optimum value is obtained as $V_0 = 112$ MeV. As usually done, we use a short-range imaginary potential with $W_0 = 30$ MeV, $r_w = 1.0$ fm and $a_w = 0.3$ fm to simulate the compound nucleus formation. Finally, the target radius is taken to be $R_T = 1.06A_T^{1/3}$. We use the same values for the parameters $\beta_2, \beta_3, N, \chi_2, \chi_{2f}$, and χ_3 as in Ref. [15]. All the calculations presented below are performed at $\theta_{\text{c.m.}} = 170^\circ$.

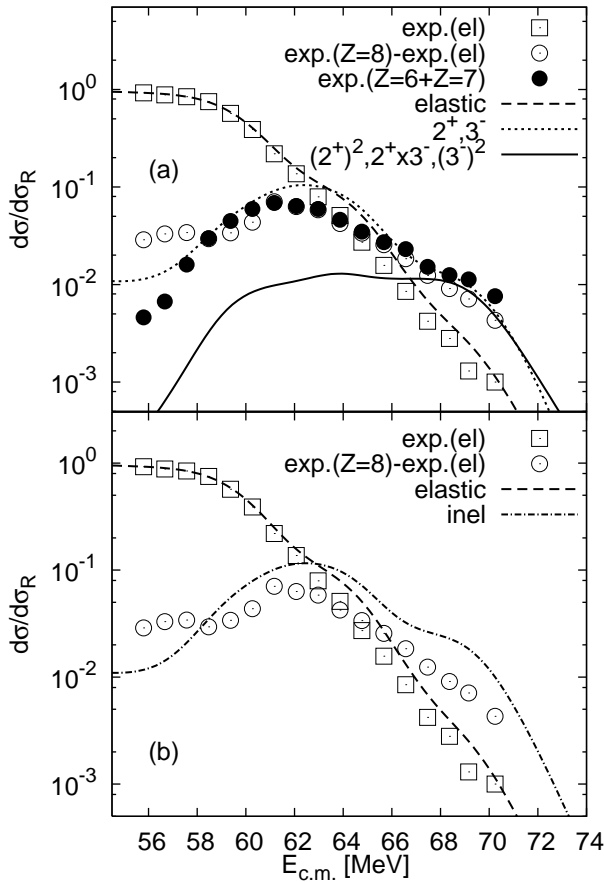


FIG. 3: (a) Comparison of the measured pure elastic (the open squares), the $Z = 8$ (–el) (the open circles) and the residual (the filled circles) components of $d\sigma_{\text{qel}}/d\sigma_R$ with the coupled-channels calculations for $^{16}\text{O}+^{144}\text{Sm}$ reaction. The $Z = 8$ (–el) component is defined as the $Z = 8$ yields subtracted the elastic component, while the residual component the sum of $Z = 6$ and 7 yields. The dashed line is the result of elastic scattering, while the dotted line shows the inelastic cross sections for the single 2^+ and 3^- phonon states. The solid line is the result of the sum of inelastic cross sections for the double phonon states in ^{144}Sm . (b) The same as (a) but for the pure elastic and the total inelastic cross sections. The experimental data are taken from Ref. [11].

The results of the coupled-channels calculations are compared with the experimental data in Fig. 2. Figures 2(a) and 2(b) show the ratio of the quasi-elastic to the Rutherford cross sections, $d\sigma_{\text{qel}}/d\sigma_R$, and the quasi-elastic barrier distributions, D^{qel} , respectively. The dotted line denotes the result in the harmonic limit, where coupling to the quadrupole and octupole vibrations in ^{144}Sm are truncated at the single phonon level, *i.e.*, only the 2^+ and 3^- states are taken into account and all the χ parameters in Eq.(5) are set to be zero. As we see this calculation fails to reproduce the experimental data. The obtained quasi-elastic cross sections, $d\sigma_{\text{qel}}/d\sigma_R$, drop much faster than the experimental data at high energies. Also the quasi-elastic barrier distribution, D^{qel} ,

exhibits a distinct peak at energy around $E_{\text{c.m.}} = 65$ MeV. These results are similar to the one achieved in Ref. [11]. The dashed line represents the result when the coupling to the quadrupole and octupole vibrations of ^{144}Sm is truncated at the double phonon states in the harmonic limit. In this case, we take into account the couplings to the 2^+ , 3^- , $2^+ \otimes 2^+$, $2^+ \otimes 3^-$ and $3^- \otimes 3^-$ states. It is obvious that the results are inconsistent with the experimental data. To see the effect of anharmonicities of the vibrations, we then perform the the same calculations using the coupling matrix elements given in Eq.(5). The resultant quasi-elastic excitation function and the quasi-elastic barrier distribution are shown by the solid line. The calculated ratio of quasi-elastic to Rutherford cross sections quite well agree with the experimental data. This suggests that the inclusion of anharmonic effects in the vibrational motions is important for the description of the quasi-elastic excitation functions for the $^{16}\text{O}+^{144}\text{Sm}$ reaction. On the other hand, the result for D^{qel} is still similar to the barrier distribution obtained by assuming the harmonic limit truncated at the one phonon level (the dotted line), although the former has a more smooth peak.

Figure 3 shows the decomposition of the quasi-elastic cross sections to each channel for the calculation with the coupling to the double anharmonic vibrations (the solid line in Fig. 2). The fraction of cross section for each channel i in the quasi-elastic cross section, $d\sigma_i/d\sigma_{\text{qel}} = d\sigma_i/[\sum_j d\sigma_j]$, is also shown in Fig. 4. The open squares are the experimental elastic cross section while the open circles are the measured excitation function for $Z = 8$ subtracted the contribution from the elastic channel. The latter contains not only the neutron transfer components but also the contributions of inelastic cross sections. The filled circles are the experimental residual (a sum of $Z = 7$ and $Z = 6$ yields) components of the $d\sigma_{\text{qel}}/d\sigma_R$. The dashed line shows results of the coupled-channels calculations for the elastic channel. It reproduces reasonably well the experimental data for elastic scattering. The $Z = 8$ component of quasi-elastic cross sections is almost exhausted by the single phonon excitations, that is, the combined 2^+ and 3^- channels, as shown by the dotted-line in Figs. 3(a) and 4(a). The cross sections for the double phonon channels are given by the solid line in Figs. 3(a) and 4(a). These are important at energies higher than around 66 MeV. If the components of all the inelastic channels included in the calculation are summed up, we obtain the dot-dashed line in Figs. 3 (b) and 4(b).

B. Effects of proton transfer reactions

In the previous subsection we have shown that the experimental quasi-elastic cross sections can be well explained within the present coupled-channels calculations, which takes into account only the inelastic excitations in ^{144}Sm . However, the shape of quasi-elastic barrier distri-

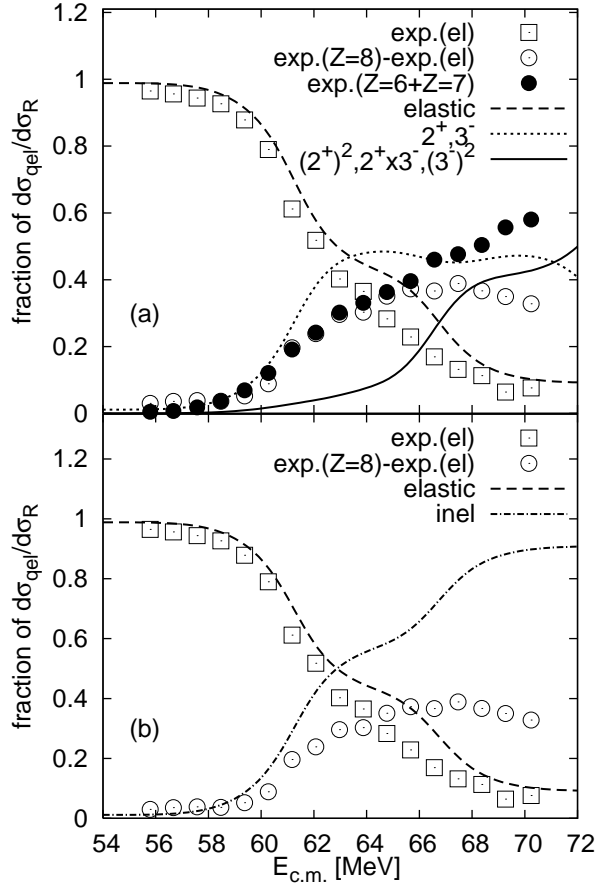


FIG. 4: Same as Fig. 3, but for the fraction of cross section for each channel in the quasi-elastic cross sections.

bution is still somewhat inconsistent with the experimental data. As one sees in Figs. 3(a) and 4(b), the experimental data indicate that the charged particle transfer reactions may also play some role (see the filled circles in the figures). In this subsection, we therefore investigate the effects of proton transfer reactions, in addition to the anharmonic double phonon excitations. To this end, we use the macroscopic form factor for the transfer coupling [21],

$$F_{\text{trans}}(r) = -F_{\text{tr}} \frac{dV(r)}{dr} \quad (6)$$

where F_{tr} is the coupling strength and $V(r)$ is the real part of the nuclear potential. In this paper, we consider a single proton transfer as well as the direct proton pair transfer reactions, although the experimental $Z=6$ component may also include the alpha-particle transfer channel. The corresponding optimum Q -values for the transfer between the ground states are $Q_{\text{opt}}(1p) = -1.79$ MeV and $Q_{\text{opt}}(2p) = 0.13$ MeV, respectively. The coupling strength F_{tr} in Eq.(6) is determined so that the experimental transfer cross sections for each $Z=6$ and $Z=7$ components [22] are reproduced. The optimum values for F_{tr} are found to be 0.12 and 0.16 fm for the one and

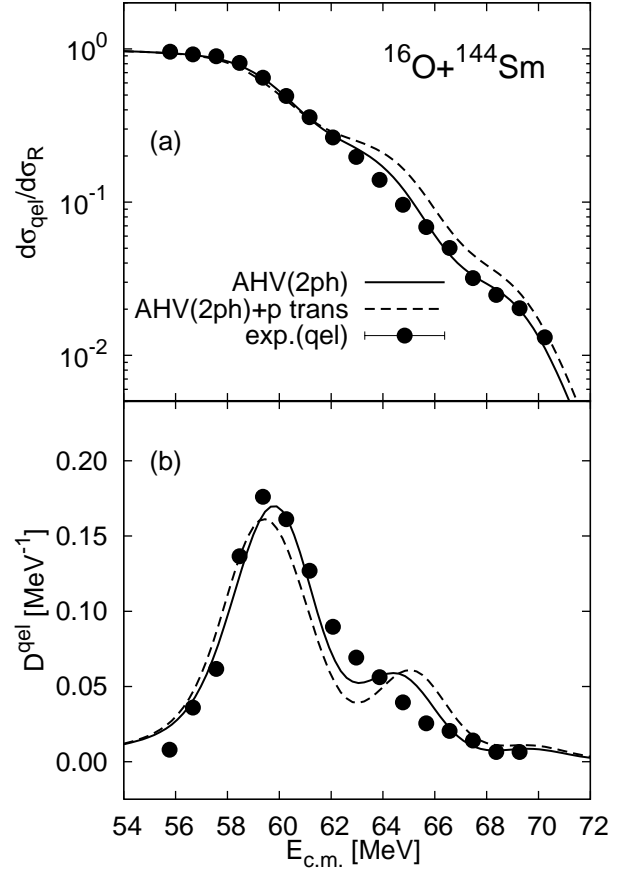


FIG. 5: Effect of proton transfers on the quasi-elastic scattering cross sections (the upper panel) and on the quasi-elastic barrier distribution (the lower panel) for $^{16}\text{O} + ^{144}\text{Sm}$ reaction. The solid line is the result of the coupled-channels calculations including the effect of double anharmonic vibrations only. The dashed line is obtained by including, in addition, the couplings to the proton transfer channels. The experimental data are taken from Ref. [11].

the two proton transfer channels, respectively.

The effects of proton transfer reactions on the quasi-elastic scattering is illustrated in Fig. 5. The solid line represents the results of the calculations including only the coupling to the double anharmonic vibrations. The dashed line is obtained by taking the coupling to the proton transfer channels into account, in addition to the anharmonic vibration channels. The upper panel shows the quasi-elastic cross sections, while the lower panel the quasi-elastic barrier distribution. We observe from Fig. 5(a) that the inclusion of proton transfer reactions overestimates the experimental $d\sigma_{\text{qel}}/d\sigma_R$ at energies between 62 and 68 MeV. Also the higher peak in the quasi-elastic barrier distribution becomes more distinct and thus worsens as compared to the calculation without the transfer channels.

Figure 6 shows the contribution of each channel to the quasi-elastic cross sections. The fraction of each contribution is also shown in Fig. 7. The open squares are

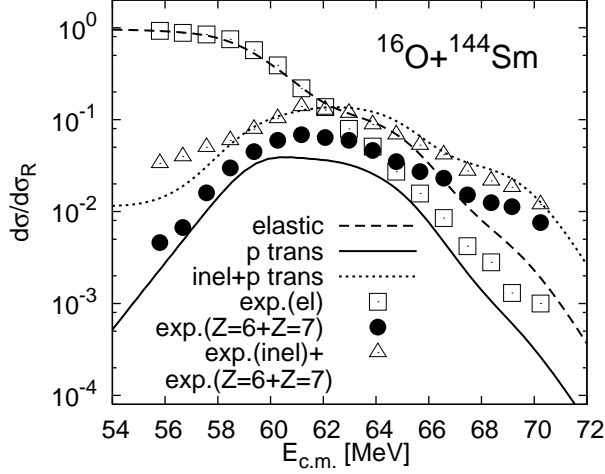


FIG. 6: Contribution of quasi-elastic cross sections from several channels. The solid and dashed line are the results of the coupled-channels calculations for the proton transfer and the elastic cross sections, respectively. The dotted line denotes the sum of total inelastic and proton transfer cross sections. The corresponding experimental data are shown by the filled circles, the open squares, and the open triangles, respectively, which are taken from Ref. [11].

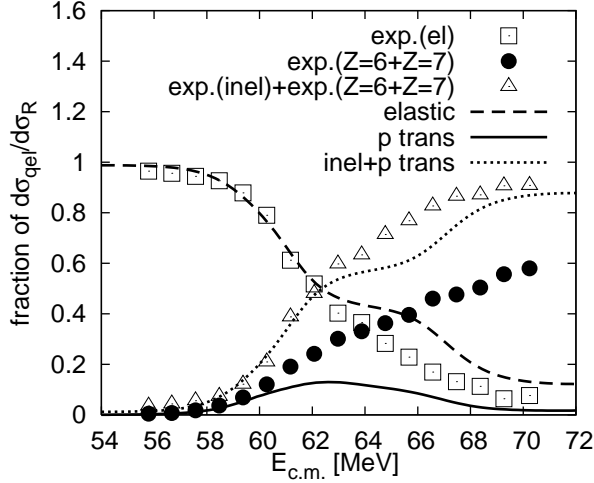


FIG. 7: Same as Fig. 6, but for the fraction in the quasi-elastic cross sections.

the experimental elastic cross sections, while the filled circles and the open triangles are the experimental proton transfer cross sections and the sum of total inelastic and transfer cross sections, respectively. The coupled-channels calculations for the elastic cross sections are shown by the dashed-line. Although it reproduces the experimental data below around 62 MeV, it overestimates the data at higher energies. The sum of the contributions from the total inelastic and the proton transfer channels is denoted by the dotted line, which reproduces the experimental data reasonably well, although the proton

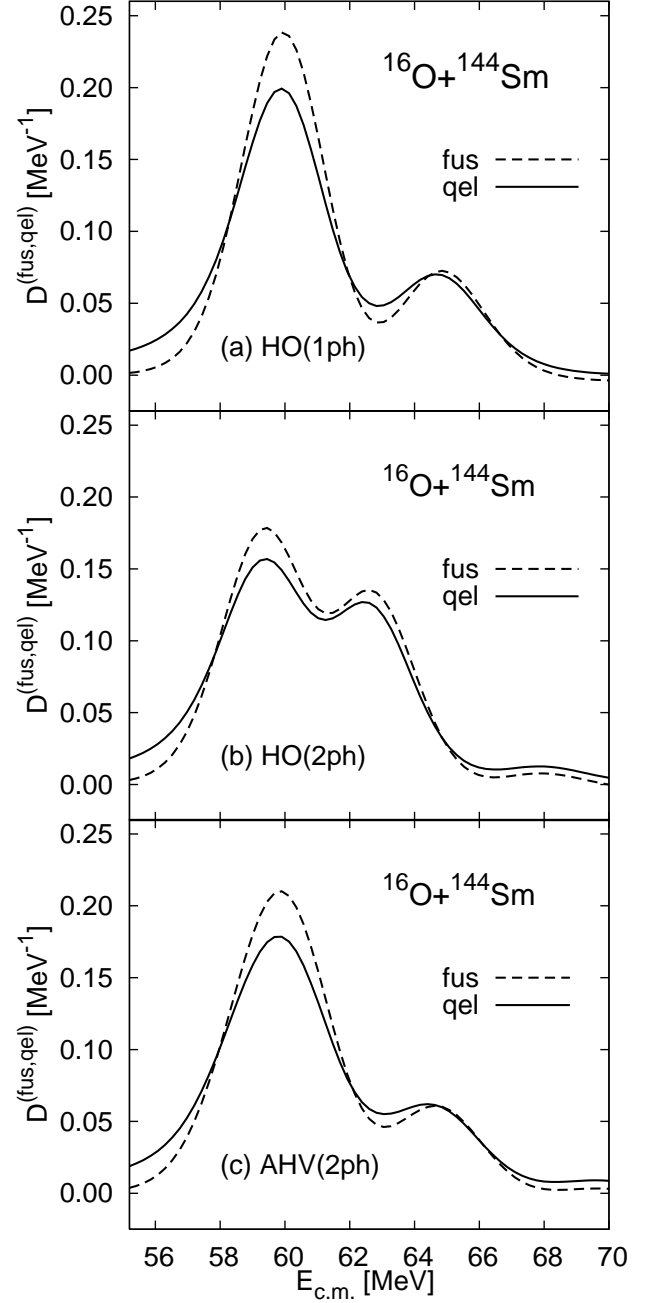


FIG. 8: Comparison of the theoretical fusion barrier distribution (dashed line) with the quasi-elastic barrier distribution (solid-line) obtained with different coupling schemes for $^{16}\text{O}+^{144}\text{Sm}$ system. Both functions are normalized to unit area in energy interval between 54 and 70 MeV. (a) The results of the coupling to one phonon state of quadrupole and octupole excitations of ^{144}Sm in the harmonic oscillator limit. (b) The same as (a) but for the coupling up to double phonon states. (c) The result when the coupling to anharmonic vibration of double quadrupole and octupole excitations in ^{144}Sm is taken into account.

transfer cross sections themselves are underestimated at energies larger than 60 MeV (the solid line). The overestimation of the quasi-elastic cross section indicated in Fig. 5(a) is therefore largely due to the contribution of elastic channel.

From this study, we conclude that the inclusion of the proton transfer reactions in the coupled-channels calculations does not explain the difference of the shape between the fusion and quasi-elastic barrier distributions for the $^{16}\text{O}+^{144}\text{Sm}$ system.

C. Discussions

We have argued that the presence of high energy shoulder, instead of high energy peak, in the quasi-elastic barrier distribution for the scattering between ^{16}O and ^{144}Sm nuclei cannot be accounted for within the present coupled-channels calculations, which take into account the anharmonic double phonon excitations in ^{144}Sm as well as the proton transfer channels. Figure 8 compares the calculated fusion barrier distribution D^{fus} and the corresponding quasi-elastic barrier distribution D^{qel} for several coupling schemes as shown in Fig. 2 in the coupled-channels calculations. The solid line shows the quasi-elastic barrier distribution while the dashed line is for the fusion barrier distribution. They are normalized so that the energy integral between 54 and 70 MeV is unity. Figures 8(a) and 8(b) are obtained by including the one phonon and the two phonon excitations in ^{144}Sm in the harmonic limit, respectively. Figure 8(c) is the result of the double anharmonic vibration coupling. From these figures, it is evident that the theoretical fusion and quasi-elastic barrier distributions are always similar to each other within the same coupling scheme, although the latter is slightly more smeared due to the low-energy tail [12]. This would be the case even with the excitations in ^{16}O as well as neutron transfer channels, which are not included in the present coupled-channels calculations. Therefore, it seems unlikely that the experimental fusion and quasi-elastic barrier distributions can be explained simultaneously within the standard coupled-

channels approach.

IV. CONCLUSION

We have studied the effects of double anharmonic vibrations of the ^{144}Sm nucleus on the large angle quasi-elastic scattering for $^{16}\text{O}+^{144}\text{Sm}$ system. We have shown that the experimental data for the quasi-elastic scattering cross sections for this reaction can be reasonably well explained. However, we found that the obtained quasi-elastic barrier distribution still shows the clear doubled-peaked structure, that is not seen in the experimental data. This was not resolved even if we took the proton transfer channels into account. Our coupled-channels calculations indicate that, within the same coupling scheme, the quasi-elastic and fusion barrier distributions are always similar to each other. Although detailed analyses including neutron transfer channels in a consistent manner are still necessary, it is thus unlikely that the fusion and quasi-elastic barrier distributions can be explained simultaneously with the standard coupled-channels framework. This fact might be related to the large diffuseness problem in sub-barrier fusion, in which dynamical effects such as couplings to deep-inelastic scattering are one of the promising origins [23, 24, 25]. It is still an open problem to perform the coupled-channels calculations with such dynamical effects and explain the difference of the shape between the fusion and the quasi-elastic barrier distributions for the $^{16}\text{O}+^{144}\text{Sm}$ reaction.

Acknowledgments

This work was partly supported by The 21st Century Center of Excellence Program “Exploring New Science by Bridging Particle-Matter Hierarchy” of Tohoku University and partly by Monbukagakusho Scholarship and Grant-in-Aid for Scientific Research under the program number 19740115 from the Japanese Ministry of Education, Culture, Sports, Science and Technology.

-
- [1] M. Beckerman, Rep. Prog. Phys., **51**, 1047 (1988).
 - [2] A.B. Balantekin and N. Takigawa, Rev. Mod. Phys. **70**, 77 (1998).
 - [3] M. Dasgupta, D.J. Hinde, N. Rowley and A.M. Stefanini, Annu. Rev. Part. Sci. **48**, 401 (1998).
 - [4] H. Esbensen, Nucl. Phys. **A352**, 147 (1981).
 - [5] M.A. Nagarajan, A.B. Balantekin and N. Takigawa, Phys. Rev. **C34**, 894 (1986).
 - [6] K.Hagino, N. Takigawa, J.R. Bennet and D.M. Brink, Phys. Rev. **C51**, 3190 (1995).
 - [7] N. Rowley, G.R. Satchler and P.H. Stelson, Phys. Lett. **B254**, 25 (1991).
 - [8] M. Dasgupta, D.J. Hinde and K. Hagino, Nucl. Phys. **A630**, 78 (1998).
 - [9] J.R. Leigh, M. Dasgupta, D.J. Hinde, J.C. Mein, C.R. Morton, J.P. Lestone, J.O. Newton, H. Timmers, J.X. Wei and N. Rowley, Phys. Rev. **C52**, 3151 (1995).
 - [10] M.V. Andres, N. Rowley, and M.A. Nagarajan, Phys. Lett. **202B**, 292 (1988).
 - [11] H. Timmers, J.R. Leigh, M. Dasgupta, D.J. Hinde, R.C. Lemon, J.C. Mein, C.R. Morton, J.O. Newton and N. Rowley, Nucl. Phys. **A584**, 190 (1995).
 - [12] K.Hagino and N. Rowley, Phys. Rev. **C69**, 054610 (2004).
 - [13] J. Raynal, *Computing as a language of Physics* (I.A.E.A., Vienna, 1972), p. 281.

- [14] H. Esbensen and B. B. Back, Phys. Rev. **C54**, 3109 (1996).
- [15] K. Hagino, N. Takigawa and S. Kuyucak, Phys. Rev. Lett. **79**, 2943 (1997).
- [16] K. Hagino, S. Kuyucak and N. Takigawa, Phys. Rev. **C57**, 1349 (1997).
- [17] K. Hagino, N. Rowley and A.T. Kruppa, Comput. Phys. Commun. **123**, 143 (1999).
- [18] A.B. Balantekin, J.R. Bennett and S. Kuyucak, Phys. Rev. **C48**, 1269 (1993); **49**, 1079 (1994) **49**, 1294 (1994).
- [19] K. Hagino *et al.* (to be published).
- [20] K. Hagino, N. Takigawa, M. Dasgupta, D.J. Hinde and J.R. Leigh, Phys. Rev. Lett. **79**, 2014 (1997).
- [21] C.H. Dasso and G. Pollarolo, Phys. Lett. **B155**, 223 (1985); C.H. Dasso and A. Vitturi, Phys. Lett. **B179**, 337 (1986).
- [22] H. Timmers, Ph.D. Thesis Australian National University, Canberra (1996)
- [23] J.O. Newton, R.D. Butt, M. Dasgupta, D.J. Hinde, I.I. Gontchar, C.R. Morton and K. Hagino, Phys. Rev. **C70**, 024605 (2004); Phys. Lett. **B586**, 219 (2004).
- [24] M. Dasgupta, D.J. Hinde, J.O. Newton and K. Hagino, Prog. Theo. Phys. Suppl. **154**, 209 (2004).
- [25] A. Mukherjee, D.J. Hinde, M. Dasgupta, J.O. Newton and R.D. Butt, Phys. Rev. **C75**, 044608 (2007).